

D. RUNDE✉  
S. BRUNKEN  
C.E. RÜTER  
D. KIP

# Integrated optical electric field sensor based on a Bragg grating in lithium niobate

Institute of Physics and Physical Technologies, Clausthal University of Technology,  
38678 Clausthal-Zellerfeld, Germany

Received: 12 April 2006/Revised version: 19 July 2006  
Published online: 31 August 2006 • © Springer-Verlag 2006

**ABSTRACT** We demonstrate a new sensor concept for the measurement of oscillating electric fields that is based on Bragg gratings in  $\text{LiNbO}_3:\text{Ti}$  channel waveguides. This miniaturized sensor that works in a retroreflective scheme does not require metallic electrodes and can be directly immersed in an oscillating electric field. The electric field induces a shift of the Bragg wavelength of the reflection grating that is due to the electro-optic effect. The operating point of the sensor is chosen by adjusting the laser wavelength to the slope of the spectral reflectivity function of the grating. In this way the magnitude of an external electric field is measured precisely as the amplitude of modulated reflected light intensity by using a lock-in amplifier. The sensor principle is demonstrated by detecting low-frequency electric fields ranging from 50 V/cm to 5 kV/cm without any conducting parts of the sensor head. Furthermore, the ability of the sensor to determine the three-dimensional orientation of an external electric field by a single rotation along the waveguide direction is demonstrated.

PACS 42.40.Eq; 42.82.-m; 42.82.Et

## 1 Introduction

High-voltage sensors that are based on electro-optic sensor heads have several advantages when compared with their purely electrical counterparts, for example minimal field disturbance, low- and high-frequency operation, and immunity to electrical noise and electromagnetic interference. Furthermore, when using an integrated scheme and optical fiber pigtail they allow for both a simple and compact design as well as excellent electromagnetic isolation.

Integrated optical sensors for the measurement of static and oscillating electric fields have been realized using different concepts. A well-known configuration is an integrated Mach–Zehnder interferometer [1] in a material like lithium niobate ( $\text{LiNbO}_3$ ), which provides large electro-optic effects [2] as well as well-established methods for the fabrication of waveguide structures [3]. Whereas a standard Mach–Zehnder interferometer requires additional metallic electrodes and appropriate biasing to obtain a linear sensor

output, more advanced schemes without any metallic parts based on reversed ferroelectric poling of the two interferometer arms have been shown [4]. Alternative designs may be based on electro-optically tuned directional couplers [5], cut-off modulators [6], Fabry–Pérot cavities [7], or field-induced phase changes of TE/TM modes in channel waveguides [8]. Whereas all the above sensor designs require input and output optical fibers on both sides of the sensor element, an improved scheme using a  $y$ -junction Mach–Zehnder interferometer has been demonstrated recently that uses a retroreflective scheme [9].

In this letter we describe a new sensor concept that combines several of the advantages of the methods described above. It is a miniaturized retroreflective sensor that does not require conducting parts, provides a linear output, and the sensitivity of the sensor can be tailored over a large range. The sensor uses a Bragg grating that is holographically recorded to reflect light at wavelengths around 1.5  $\mu\text{m}$  in a single-mode channel waveguide in  $\text{LiNbO}_3$  [10]. Due to the linear electro-optic effect, the spectrum of Bragg-reflected light is linearly shifted as a function of electric field. Thus, for a fixed wavelength adjusted to an operating point in the slope of the reflectivity spectrum, the change in the grating reflectivity provides a linear sensor output.

Refractive index Bragg gratings in  $\text{LiNbO}_3$  channel waveguides can be holographically recorded using the photorefractive effect. Recently, we have demonstrated the suitability of such gratings for operation at telecommunication wavelengths around 1.5  $\mu\text{m}$  [10, 11], which may be used as spectral filters, e.g. for applications like dense wavelength division multiplexing (DWDM). Here, the suitability of such gratings for the detection of external electric fields is demonstrated.

## 2 Sensor principle

The sensor utilizes the strong wavelength dependence of the reflectivity at the slope of the reflection spectrum of a narrow-bandwidth Bragg grating. A scheme of the sensor's operating principle is shown in Fig. 1. Let us assume a Bragg grating of period  $\Lambda = \lambda_B / (2n_{\text{eff}})$  with peak reflection wavelength  $\lambda_B$  in an electro-optic waveguide with effective mode refractive index  $n_{\text{eff}}$ . An electric field induces a Bragg-wavelength shift due to the electro-optic effect,  $\Delta\lambda_B = n_{\text{eff}}^3 r_{\text{eff}} \Delta E$ , where  $r_{\text{eff}}$  is the effective electro-optic

✉ Fax: +49-5323-72-2175, E-mail: daniel.runde@tu-claustal.de

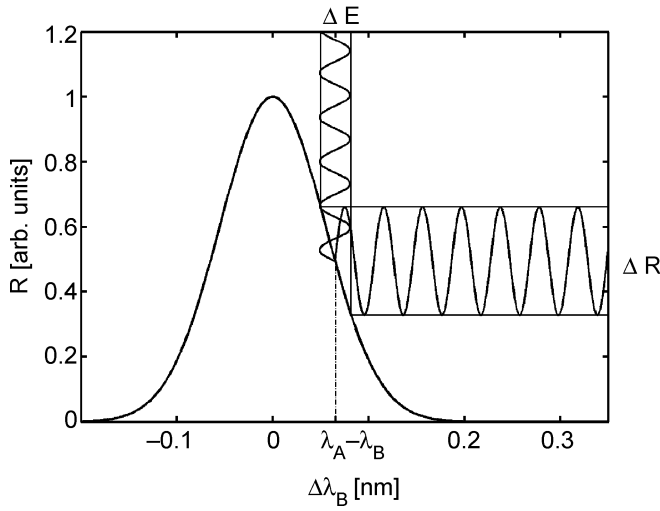


**FIGURE 1** Sensor principle. The laser wavelength is locked at the operating point  $\lambda_A$  to provide a constant sensitivity  $\partial R/\partial\lambda$ . An applied oscillating electric field  $\Delta E$  results in a proportional change of reflectivity  $\Delta R$

coefficient and  $\Delta E$  is the amplitude of the applied electric field [12]. The laser wavelength is set to an operating point  $\lambda = \lambda_A$  at the slope of the reflection peak; see Fig. 1. At this point, a modulated electric field causes a proportional (modulated) change of the reflectivity of the grating. With the help of a lock-in amplifier locked to the frequency of the oscillating electric field, this change can be measured precisely in the back-reflected light. Formally, the reflectivity dependence on the applied electric field can be described in the form

$$\Delta R = \frac{\partial R}{\partial E} \Delta E. \quad (1)$$

This equation can be expanded to

$$\Delta R = \frac{\partial R}{\partial \lambda_B} \frac{\partial \lambda_B}{\partial n_{\text{eff}}} \frac{\partial n_{\text{eff}}}{\partial E} \Delta E. \quad (2)$$

The term  $(\partial n_{\text{eff}}/\partial E)\Delta E$  is identified as the electro-optic effect with  $\partial n_{\text{eff}}/\partial E = -0.5n^3 r_{\text{eff}}$ . Since  $R$  depends on  $\lambda - \lambda_B$ , we use the relation  $(\partial R/\partial \lambda_B)(\partial \lambda_B/\partial n_{\text{eff}}) = -(\partial R/\partial \lambda)(\partial \lambda_B/\partial n_{\text{eff}})$ . With the Bragg condition  $\Delta \lambda_B = 2\Lambda \Delta n_{\text{eff}}$ , the electric field amplitude is finally described by

$$\Delta E = \Delta R \left( \frac{\partial R}{\partial \lambda} \right)^{-1} \frac{1}{n^3 \Lambda r_{\text{eff}}}. \quad (3)$$

The change  $\Delta B$  of the inverse dielectric tensor as a function of the electric field  $E$  can be expressed in the form [2]

$$\Delta B_{ij} = \begin{pmatrix} -r_{22}E_2 + r_{13}E_3 & -r_{22}E_1 & r_{51}E_1 \\ -r_{22}E_1 & r_{22}E_2 + r_{13}E_3 & r_{51}E_2 \\ r_{51}E_1 & r_{51}E_2 & r_{33}E_3 \end{pmatrix} \quad (4)$$

with the four independent electro-optic tensor elements  $r_{12} = -r_{22} = r_{61}$ ,  $r_{51} = r_{42}$ ,  $r_{13} = r_{23}$ , and  $r_{33}$  for LiNbO<sub>3</sub> with point group symmetry  $3m$ . For light traveling in the channel waveguides along the  $c$  axis the normalized dielectric displacement splits into two polarization directions,  $d_{\text{TE}} = (0, 1, 0)$  for TE and  $d_{\text{TM}} = (1, 0, 0)$  for TM.

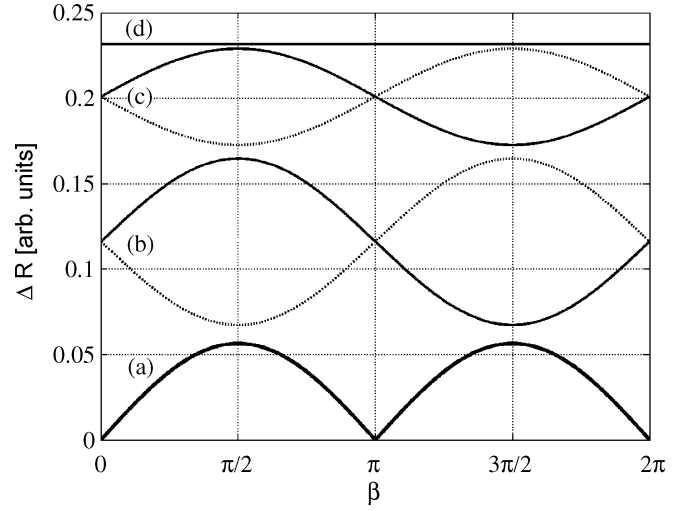


**FIGURE 2** Calculated modulated reflectivity  $\Delta R$  as a function of rotation angle  $\beta$  in the  $xy$  plane for different orientations  $(\varphi, \theta)$  of the external electric field and fixed parameters  $\partial R/\partial E = 9.7 \times 10^{-8} \text{ W}/(\text{kV}/\text{cm})$  and  $E = 3 \text{ kV}/\text{cm}$ : (a)  $\varphi_0 = 0, \theta_0 = \pi/2$  (thick solid line); (b)  $\varphi_0 = 0, \theta_0 = \pi/3$  (dotted line) and  $\theta_0 = 2\pi/3$  (solid line); (c)  $\varphi_0 = 0, \theta_0 = \pi/6$  (dotted line) and  $\theta_0 = 5\pi/6$  (solid line); and (d)  $\varphi_0 = 0, \theta_0 = \pi$  (solid line). Orientations  $(\theta, \pi - \theta)$  differ only by a phase shift  $\Delta\beta = \pi$

By defining the electric field in spherical coordinates  $\mathbf{E} = E(\sin\theta \cos\phi, \sin\theta \sin\phi, \cos\theta)$ , where  $\theta$  is the angle to the positive  $c$  axis and  $\phi$  the angle in the  $xy$  plane to the positive  $x$  axis, we obtain

$$\begin{aligned} \Delta B_{\text{TM}} &= \langle d | \Delta B | d \rangle = E(-r_{22} \sin\theta \sin\phi + r_{13} \cos\theta), \\ \Delta B_{\text{TE}} &= \langle d | \Delta B | d \rangle = E(r_{22} \sin\theta \sin\phi + r_{13} \cos\theta). \end{aligned} \quad (5)$$

Notice that the coordinate system  $(x, y, z)$  is fixed to the crystal axes. Using  $\langle \Delta B \rangle = r_{\text{eff}} E$ , we obtain the effective electro-optic coefficient

$$\begin{aligned} r_{\text{eff, TM}} &= -r_{22} \sin\theta \sin\phi + r_{13} \cos\theta, \\ r_{\text{eff, TE}} &= r_{22} \sin\theta \sin\phi + r_{13} \cos\theta, \end{aligned} \quad (6)$$

which depends on both the field orientation and the light polarization. Given the sensor sensitivity  $\partial R/\partial E$ , for each polarization of the guided light (either TE or TM) a single rotation of the sensor element in the  $xy$  plane provides the full information of the orientation of the external electric field, i.e. it allows for the determination of the two angles  $\theta$  and  $\phi$ . Typical examples for different field orientations  $(\theta, \phi)$  are given in Fig. 2.

In the bulk material the electric field amplitude is decreased by the dielectric constant  $\varepsilon$  for the relevant direction, where for LiNbO<sub>3</sub> we have  $\varepsilon_x = \varepsilon_y = 84$  and  $\varepsilon_z = 30$  [2]. However, to account for only partial screening of the external electric field directly at the surface (waveguide) layer of the sample, an additional correction factor  $f$  may be used when comparing experimentally obtained values for  $E$  with theory. This factor is introduced later in Sect. 4.

### 3 Sensor fabrication

Crystal samples of  $20 \times 7.8 \times 1 \text{ mm}^3$  are cut from  $x$ - or  $y$ -cut wafers of congruently melting LiNbO<sub>3</sub>. The  $c$

axis is parallel to the 20-mm edge. Several 6- $\mu\text{m}$ -wide single-mode channel waveguides are fabricated parallel to the  $c$  axis by in-diffusion of 100-nm-thick titanium stripes. The diffusion takes place at 1273 K for 18 h in air. To increase the photorefractive sensitivity of  $\text{LiNbO}_3$ , the diffusion is followed by the evaporation of a 83-nm-thick copper layer and a second diffusion step for 2 h at 1273 K in a reducing wet argon atmosphere to increase the proton concentration in the waveguide region [12, 13].

To record a grating in transmission geometry the waveguide sample is placed in the interference region of a two-beam interference setup using the green line of an argon-ion laser at wavelength  $\lambda_S = 514.5 \text{ nm}$  [11]. The setup allows precise adjustment of the angle  $2\varphi$  between the two beams, which is related to the desired Bragg wavelength  $\lambda_R$  by  $\varphi = \arcsin(\lambda_S n_{\text{eff}}/\lambda_R)$ . Typical values of the grating length and amplitude of the recorded refractive-index change are  $s_0 \approx 15 \text{ mm}$  and  $\Delta n \approx 1 \times 10^{-4}$ , respectively. To allow for constant phase relations of the writing beams during recording, an active phase stabilization system is used [12, 14]. A significantly increased lifetime of the holograms to tens of years can be obtained by thermal fixing [15, 16]. For this, the sample is heated to a temperature of 453 K during the recording process. At these elevated temperatures positive ions like hydrogen become mobile and drift in the electronic space charge field [17]. After recording and cooling to room temperature, a homogeneous illumination of the sample leads to a partial redistribution of the electrons and a strong grating occurs due to the ionic charges, which cannot be erased by visible light. Finally, an optical single-mode fiber is adjusted and glued to the polished end face for coupling light into the channel waveguide.

The test setup for the detection of electric fields is depicted in Fig. 3. The sensor is held between two plates of a capacitor which provides a homogeneous electric field in the sensor region. The capacitor is mounted on a rotatable holder which allows for an independent orientation of the field direction relative to the fixed sensor head. The light from a tunable distributed feedback laser (DFB) laser with a wavelength range  $\lambda = 1.52\text{--}1.63 \mu\text{m}$  and a spectral line width below 150 kHz is coupled into a single-mode fiber and split into two parts by a  $2 \times 2$  coupler. One part is guided to a photodetector (PD) to monitor the laser power whereas the other part is coupled into the sensor. A polarization controller allows for choosing the correct light polarization to excite either TE or TM modes of the channel waveguide. The light reflected from the grating passes the  $2 \times 2$  coupler and is measured by a second pho-

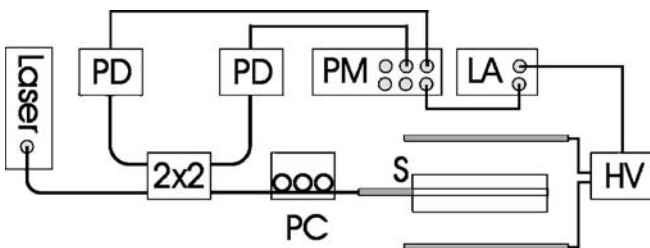


**FIGURE 3** Experimental scheme for testing the sensor: PDs, photodiodes; PM, optical power meter;  $2 \times 2$ , 3 dB coupler; PC, polarization controller; LA, lock-in amplifier; S, sensor head; HV, high-voltage amplifier

todetector that is connected to a lock-in amplifier. The lock-in amplifier is synchronized to the AC field that is applied to the capacitor by a high-voltage amplifier. The strength of the field  $E$  can be additionally adjusted by changing the distance  $l$  of the parallel plates of the capacitor.

#### 4 Sensor properties

In Fig. 4 the reflectivity spectrum for TE-polarized light of a grating recorded into the  $x$ -cut sample  $x-1$  is shown. The operating point is set to about half the maximum position at  $P = 3.5 \times 10^{-6} \text{ W}$  on the left-hand slope of the peak by adjusting the wavelength of the DFB laser. Here the corresponding linear slope efficiency is  $\partial R/\partial \lambda = 3.7 \times 10^{-4} \text{ W/nm}$ , which can be further tailored over a larger range by varying the grating length  $s_0$  and amplitude  $\Delta n$ .

When the sensor head is placed in the oscillating electric field the modulated reflectivity  $\Delta R$  can be measured versus the electric field amplitude  $E = E_y$ . The direction of the electric field in this measurement points along the  $y$  axis of the sample, i.e. it is tangential to the sensor surface and perpendicular to the  $c$  axis. In Fig. 5 the linear dependence of the reflected signal  $\Delta R$  on the applied field strength  $E$  is presented. From this measurement we obtain a sensitivity of  $\partial R/\partial E = 9.7 \times 10^{-8} \text{ W/(kV/cm)}$ . For the detector used minimum measurable field strengths of 50 V/cm are obtained, while the maximum field amplitude of 5.6 kV/cm is limited only by the high-voltage amplifier used (10 kV peak-to-peak voltage) and a minimal distance of the capacitor of  $l \sim 1 \text{ cm}$ . When comparing the experimentally obtained sensitivity with the theoretical model from (3) and (6) and using  $r_{22} = 6.8 \text{ pm/V}$  [2], we find that the field sensed by the guided light is higher by a factor  $f = 9.59$  compared to the field  $E_{\text{bulk}}$  inside the bulk ( $E_{\text{bulk}} = E_y/\varepsilon_y$  with  $\varepsilon_y = 84$ ).

The ability of the sensor concept to determine the orientation of an external field in three dimensions is demonstrated

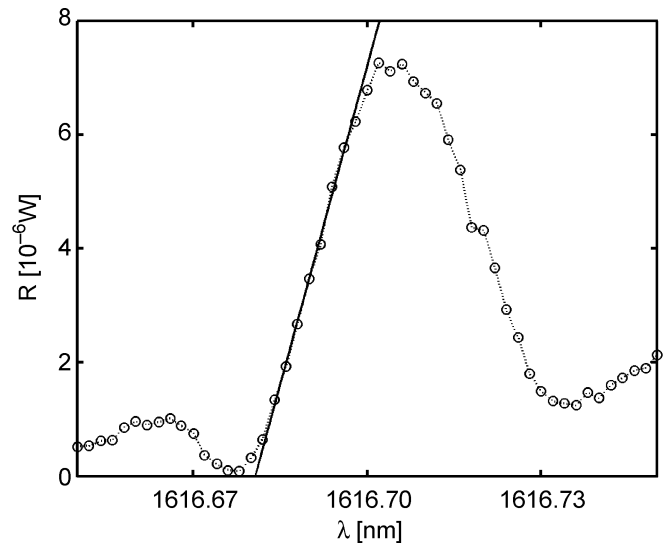


**FIGURE 4** Reflection spectrum of the Bragg grating in sample  $x-1$  with a bandwidth (FWHM) of about 50 pm. The slope at the operating point ( $P = 3.5 \times 10^{-6} \text{ W}$ ) of the half-maximum position on the *left-hand side* is  $\partial R/\partial \lambda = 3.7 \times 10^{-4} \text{ W/nm}$

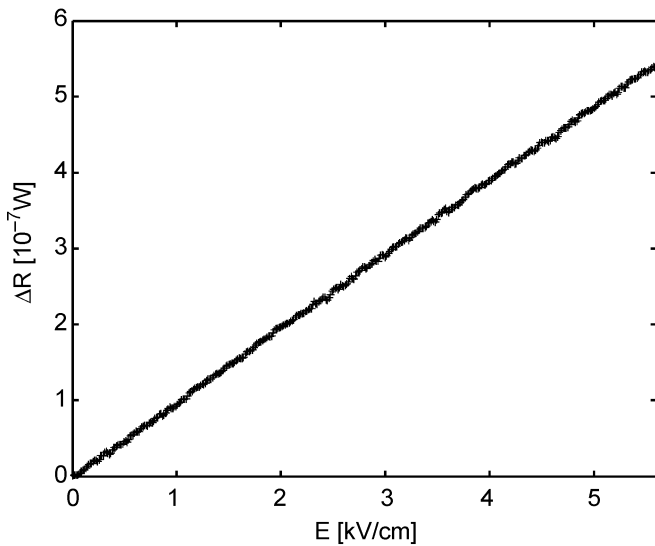


**FIGURE 5** Measured intensity modulation  $\Delta R$  versus the applied electric field  $E$ . A linear fit to the measured slope results in a sensor sensitivity of  $\partial R/\partial E = 9.7 \times 10^{-8} \text{ W}/(\text{kV}/\text{cm})$

in the next experiment, where we again use the  $x$ -cut sample  $x - 1$  and TE-polarized light. For simplicity we use a constant electric field  $E = 2.83 \text{ kV}/\text{cm}$ , perpendicular to the sample's  $c$  axis, that is rotated by an angle  $\beta$  in the  $xy$  plane of the LiNbO<sub>3</sub> crystal, where  $\beta = 0$  corresponds to the  $+x$  direction (see curve (a) in Fig. 2). The measured reflectivity modulation as a function of rotation angle  $\beta$  as well as a fit to the theoretical dependence (solid line, where, as described above, a correction factor  $f = 9.98$  has to be used for the tangential field component  $E_y$ ) are given in Fig. 6. For  $\beta = 0$  and  $\beta = \pi$  no signal is obtained, as can be seen from (5) where the  $x$  component of the applied electric field vanishes. This is due to the fact that  $r_{21} = 0$  for LiNbO<sub>3</sub>. Therefore, the expected result of this measurement is a field orientation  $\varphi_0 = 0$  and  $\theta_0 = \pi/2$ . Note that only the orientation but not the polarity of the field is detected; thus, the fit parameters  $\varphi_0 = 0$  and

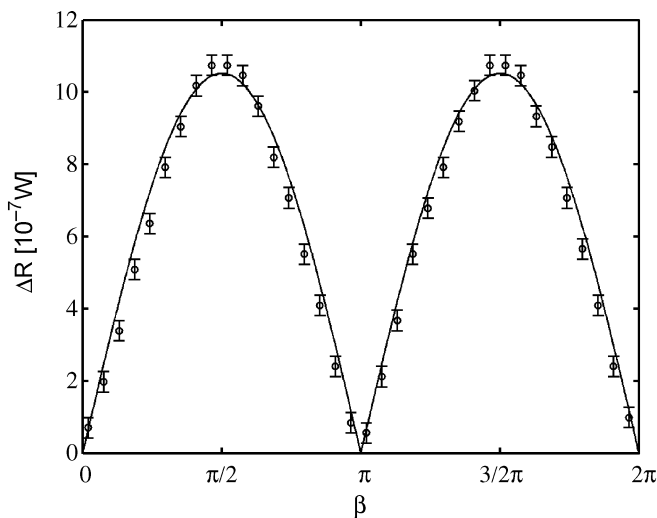


**FIGURE 6** Measured intensity modulation  $\Delta R$  versus rotation angle  $\beta$  in the  $xy$  plane of the sensor sample immersed in an electric field. From the theoretical fit a field orientation  $\varphi_0 = 0$ ,  $\theta_0 = \pi/2$  is obtained

$\varphi_0 = \pi$  are of equal value here. When the external field has an additional component along the sample's  $c$  axis, the curve in Fig. 6 is additionally shifted vertically due to the influence of the tensor element  $r_{113} = 10.8 \text{ pm}/\text{V}$ , which allows for the determination of the angle  $\theta$ .

As a result of multiple measurements we find that the tangential field components are increased by an averaged factor  $\bar{f} = 9.6 \pm 0.9$  when compared to the expected bulk value. On the other hand, measurements using  $y$ -cut sensor samples and  $E = E_y$  show that for fields perpendicular to the sensor surface no correction factor has to be applied.

As a result of Maxwell's equations, boundary conditions require that normal electric field components show a step-like dependence at the sample surface,  $E_{\text{bulk}} = E/\epsilon$ , whereas for tangential components the internal field has to match the external field at the dielectric boundary. Consequently, within a thin boundary layer the external field  $E$  gradually decreases to the bulk value  $E/\epsilon$  inside the sample, where the thickness of this layer is related to the Debye screening length, i.e. to the charge density of the LiNbO<sub>3</sub> crystal.

To estimate the thickness  $\sigma$  of this layer, we use the well-known electro-optic behavior of LiNbO<sub>3</sub>. First, we use the finite-difference method to calculate the mode profiles and the propagation constant of the guided mode of our waveguide without external electric field. Next, we assume a depth dependence of the external electric field in the form  $E(y) = E((\epsilon - 1) \exp(-y/\sigma) + 1)/\epsilon$ , where the electric field exponentially decreases from the surface value  $E$  at  $y = 0$  to a value  $E/\epsilon$  in a depth  $\sigma$  inside the sample. Then, we calculate the electro-optically induced refractive-index change of this field that is superimposed to the waveguide refractive-index profile  $n(x, y)$ . Finally, a fit procedure allows calculating the corresponding depth parameter  $\sigma$  that matches the measured change of the effective refractive index of the guided mode. As a result, we obtain a  $1/e$  depth of  $\sigma = 1.9 \mu\text{m}$  of the electric field, corresponding to the measured correction factor  $\bar{f} = 9.6$ .

## 5 Conclusion

An integrated optical sensor was demonstrated that uses the electric field dependence of a reflection Bragg grating recorded in electro-optic LiNbO<sub>3</sub> channel waveguides. The device does not require conducting parts and works in a retroreflective scheme. The sensor has been used to measure oscillating electric fields in a range from 0.05 to 5.6 kV/cm, resulting in a linear sensitivity that may be further improved by tailoring of the spectral dependence of the written Bragg gratings. It has been shown that the electric field of tangential field components is increased by a factor of  $9.6 \pm 0.9$  close to the surface of the LiNbO<sub>3</sub> sensor head when compared with the value in the bulk of the sample, resulting in a penetration depth (screening length) of the electric field of  $1.9 \mu\text{m}$ . Furthermore, the sensor allows for measuring the three-dimensional orientation of the electric field by a single rotation of the sensor head.

**ACKNOWLEDGEMENTS** We thank the Deutsche Forschungsgemeinschaft for financial support of this research (grants KI 482/6-1 and 6-2).

## REFERENCES

- 1 N.A.F. Jaeger, L. Young, *IEEE J. Lightwave Technol.* **7**, 229 (1989)
- 2 R.S. Weis, T.K. Gaylord, *Appl. Phys. A* **37**, 191 (1985)
- 3 D. Kip, *Appl. Phys. B* **67**, 131 (1998)
- 4 D.H. Naghski, J.T. Boyd, H.E. Jackson, S. Siriam, S.A. Kingsley, J. La-tess, *J. Lightwave Technol.* **12**, 1092 (1994)
- 5 M.M. Howerton, C.H. Bulmer, W.K. Burns, *Appl. Phys. Lett.* **52**, 1850 (1988)
- 6 N.A.F. Jaeger, F. Rahmatian, *IEEE Trans. Power Deliver.* **10**, 127 (1995)
- 7 M. Huang, M. Lu, J. Shy, *Rev. Sci. Instrum.* **75**, 5364 (2004)
- 8 T. Ichiwawa, M. Kagami, H. Ito, *IEICE Trans. Electron. E* **83C**, 355 (2000)
- 9 S.-S. Lee, M.-C. Oh, S.-Y. Shin, K.-H. Keh, *IEEE Photon. Technol. Lett.* **5**, 996 (1993)
- 10 J. Hukriede, I. Nee, D. Kip, E. Krätzig, *Opt. Lett.* **23**, 1405 (1998)
- 11 J. Hukriede, D. Kip, E. Krätzig, *Appl. Phys. B* **66**, 333 (1998)
- 12 J. Hukriede, D. Runde, D. Kip, *J. Phys. D Appl. Phys.* **36**, R1 (2003)
- 13 K. Peithmann, J. Hukriede, K. Buse, E. Krätzig, *Phys. Rev. B* **61**, 4615 (2000)
- 14 P.M. Garcia, K. Buse, D. Kip, J. Frejlich, *Opt. Commun.* **117**, 235 (1995)
- 15 D.L. Staebler, J.J. Amodei, *Ferroelectrics* **3**, 107 (1972)
- 16 L. Arizmendi, E.M. Miguel-Sanz, M. Carrascosa, *Opt. Lett.* **23**, 960 (1998)
- 17 K. Buse, S. Breer, K. Peithmann, S. Kapphan, M. Gao, E. Krätzig, *Phys. Rev. B* **56**, 1225 (1997)